**Original Research**

# Manganese-Enhanced MRI in a Rat Model of Parkinson's Disease

Galit Pelled, PhD,[1,2] Hagai Bergman, MD,[3] Tamir Ben-Hur, MD, PhD,[4] and Gadi Goelman, PhD[1]*

**Purpose:** To measure intra- and inter-hemispheric connectivity within the basal ganglia (BG) nuclei in healthy and in unilateral 6-hydroxydopamine (6-OHDA) Parkinson disease rat model in order to test the BG interhemispheric connectivity hypothesis.

**Material and Methods:** The manganese-enhanced MRI (MEMRI) method with direct injection of manganese chloride into the entopeduncular (EP), substantia nigra (SN), and the Habenula nuclei in unilateral 6-OHDA ($N = 22$) and sham-operated ($N = 16$) rat groups was used. MEMRI measurements were applied before, 3, 24, and 48 hours post-manganese injection. Signal enhancements in T1-weighted images were compared between groups.

**Results:** Manganese injection into the EP nucleus resulted with bihemispheric signal enhancements in the habenular complex (Hab) at both groups with stronger enhancements in the 6-OHDA group. It also exhibited lower sensorimotor cortex signal enhancement in the 6-OHDA rat group. SN manganese injection caused enhanced anteroventral thalamic and habenular nuclei signals in the 6-OHDA rat group. Manganese habenula injection revealed enhanced interpeduncular (IP) and raphe nuclei signals of the 6-OHDA rat group.

**Conclusion:** Modulations in the effective intra- and inter-hemispheric BG connectivity in unilateral 6-OHDA Parkinson's disease (PD) rat model support the BG interhemispheric connectivity hypothesis and suggest a linkage between the dopaminergic and serotonergic systems in PD, in line with clinical symptoms.

**Key Words:** manganese-enhanced MRI; Parkinson's disease; 6-hydroxydopamine; basal ganglia; functional connectivity; rat

**Abbreviations:** PD = Parkinson's disease, 6-OHDA = 6-hydroxydopamine, BG = basal ganglia, SN = substantia nigra, SNc = substantia nigra pars compacta, MRI = magnetic resonance imaging. EP = entopeduncular nucleus, MEMRI = manganese-enhanced MRI.

**J. Magn. Reson. Imaging 2007;26:863–870.**



THE BASAL GANGLIA (BG) nuclei are known to participate in the implementation of planned and motivated behaviors that integrate motor, cognitive, and limbic functions. While it is best known for its control of movement, the BG is also involved in processes such as emotions, motivations, and cognitions that lead up to movement. Based on the functional and anatomical organization of corticostriatal pathways, it is well accepted that the BG nuclei are (fully or partially) segregated in accordance with cortical input. For example, BG ventral regions are involved in reward and participate in addictive behavior as well as habit formation (1,2); central BG areas are involved in cognitive functions such as procedural learning and working memory (3); and the dorsolateral portion of the striatum is associated with the control of movement. Moreover, diseases affecting mental health such as schizophrenia (4,5), drug addiction (6), and obsessive compulsive disorder (7) are linked to BG pathology as are diseases affecting motor control. The association with multiple neurological and psychiatric disorders manifesting themselves in the BG-cortex circuitry highlights the importance of understanding this circuit.

Several different models for this circuit were proposed, starting from the classical box-and-arrow Albin-DeLong model (8,9), through the example of parallel processing of cortical information (10). Other models include the idea of pathways allowing information from separate cortical-BG loops to influence each other (11,12), the concept of circuits that include nonreciprocal arrangements between structures (11,13), and the "reinforcement driven dimensionality reduction

[1]MRI/MRS Laboratory, Human Biology Research Center, Department of Medical Biophysics and Nuclear Medicine, Hadassah Hebrew University Medical Center, Jerusalem, Israel.

[2]Laboratory of Functional and Molecular Imaging, National Institute of Neurological Disorders and Stroke, National Institutes of Health, Bethesda, Maryland, USA.

[3]Department of Physiology, Hadassah Medical School and the Eric Roland Center for Neurodegenerative Diseases, The Hebrew University, Jerusalem, Israel.

[4]Department of Neurology, the Agnes Ginges Center for Human Neurogenetics, Hadassah Hebrew University Hospital, Jerusalem, Israel.

Contract grant sponsors: Dana Foundation; Israel Ministry of Sciences and Israel Science Foundation (Grant no. 596/01).

*Address reprint requests to: G.G., PhD, MRI/MRS lab, the Human Biology Research Center, Department of Medical Biophysics and Nuclear Medicine, Hadassah Hebrew University Medical Center, Jerusalem, Israel. E-mail: gadig@hadassah.org.il

Received May 20, 2006; Accepted 30 May 2007.

DOI 10.1002/jmri.21051

Published online in Wiley InterScience (www.interscience.wiley.com).

model" (14). In all these models, the cortex-BG-cortex circuits are treated as being in a single hemisphere neglecting its bihemispherical connections. However, recently abnormal sensorimotor activation in hemiparkinsonic patients and in the unilateral rat model of Parkinson's disease (PD) was observed bilaterally, raising the question of whether the bilateral connections of the BG affect BG circuitry.

Functional neuroimaging using positron emission tomography and functional magnetic resonance imaging (fMRI) has shown bilateral cortical activation as a response to akinetic hand stimulation in human (15) and in the unilateral PD rat model during unilateral forepaw sensory stimulation (16). This abnormal cortical response of the "healthy" hemisphere suggests strong effective connectivity between hemispheres in the parkinsonian state that could be accomplished through the cortex or, as we have hypothesis before (16), by an amplification of the BG bilateral connections. The latter mechanism is thought to be mediated by interhemispheric connections, which have been demonstrated to exist in primates, cats, and rats. The BG has two output nuclei: the globus pallidus internal segment (GPi) which is the primate homologue to the rodent entopeduncular nucleus (EP), and the SN pars reticulata (SNr). It has been demonstrated that 15% to 20% of the projections from the BG output nuclei terminate in the contralateral hemisphere (17–20). To further reveal the BG circuitry, the habenular complex (Hab), that had traditionally not been considered part of this circuitry, has received much interest lately, with the observations of its strong connections with the BG (21–23) and its involvement in PD (24).

In order to better understand BG circuitry we wished: 1) to identify the in vivo effective connectivity from the two BG output nuclei, the EP and the SNr nuclei, with the Hab complex; and 2) to compare this connectivity between normal and BG pathological states (e.g., PD) using the unilateral 6-hydroxydopamine (6-OHDA) rat model. For in vivo measurements of anterograde connectivity, we used the manganese-enhanced MRI (MEMRI) method. In this method, manganese ions ($Mn^{2+}$), which are paramagnetic and thus detectable by MRI, are directly injected into the brain. Due to the chemical and physical similarity of the $Mn^{2+}$ to calcium ions, manganese ions are thought to enter neurons through voltage gated calcium channels, move in an anterograde manner along axons and cross synapses (25). Manganese uptake has shown to be highly correlated with neuronal activity (25–29). In recent years, MEMRI methods have been applied to study functional and structural connectivity in birds (30,31), rodent (32–34), and monkeys (29,35).

## MATERIALS AND METHODS

All surgical and experimental procedures were conformed and approved by the Animal Care committee guidelines.

A total of 22 male Sprague-Dawley rats weighing 250–300 g were anesthetized with ketamine (90 mg/kg intraperitoneally [i.p.]; Sigma, Israel) and xylazine (5 mg/kg i.p.; Sigma) and stereotaxically injected into the right substantia nigra pars compacta (SNc) with 4 μL of 10 mM 6-OHDA hydrochloride with 0.01% ascorbic acid (Sigma), using a 10-μL Hamilton microsyringe fitted with a 26-gauge cannula. The injection rate was 1 μL/minute and the cannula was left in place for an additional five minutes. Lesion coordinates for SNc lesion were anterior-posterior (AP)-4.8; medial-lateral (ML)-1.6, dorsal-ventral (DV)-8.4 from the dura, according to a rat brain atlas (36). For the control group, an additional 16 rats went through the same surgical procedure, but were injected with 4 μL of saline to the SNc (sham-operated rats).

Two weeks after the 6-OHDA lesion procedure, 0.3 μl of 0.16 M manganese chloride ($MnCl_2$, dissolved in saline) solution was injected directly to the right EP (AP-2.3, ML-2.6, DV-7.5 from dura; six right-SNc-6-OHDA and six right-SNc-sham-operated rats) or to the right SNr (AP-5.3, ML-2.8, DV-8.5 from dura; five right-SNc-6-OHDA and five right-SNc-sham-operated rats). Due to the small volume of the Hab, injections to the right Hab (AP-2.5, ML-0.8, DV-4.4 from dura; seven right-SNc-6-OHDA and five right-SNc-sham-operated rats) were performed with 0.1 μL of 0.04 M $MnCl_2$. The $MnCl_2$ injection rate was 0.05 μL/minute, and the cannula was left in the injection sites for an additional seven minutes. Three hours post $MnCl_2$ injection rats were imaged to ensure that the injection areas were in place and comparable. Manual inspection revealed no differences between animals within or between groups. Although we attempted to inject the $MnCl_2$ exclusively into the injection targets, we refer to them here as the EP, SN, and Hab areas, respectively, due to the possibility of manganese diffusion to their vicinity.

Using the average rate of axonal manganese ($Mn^{2+}$) transport calculated in rats (2 mm/hour) (37), we estimated that 48 hours will be sufficient for most $Mn^{2+}$ transportation of interest in this study. A total of four MEMRI sessions were performed on each animal using a 4.7 T Biospec system (Bruker Biospin MRI Gmbh, Ettlington, Germany), one before $MnCl_2$ injection and at 3, 24, and 48 hours post injection. Rats were anesthetized with isoflurane (2% with a mixture of 30:70 $O_2$:$N_2O$) and were restrained in a home-built head and body holder. Body temperature was kept at 37°C, using a heating pad. MRI measurements were performed with a 38-mm Bruker head-dedicated volume coil. For MEMRI studies, T1 weighted images using a gradient-echo sequence was applied to obtain coronal slices (TR = 156 msec, TE = 6.7 msec, matrix size = 256 × 128, zero-filled to 256 × 256, field of view = 3 cm, flip angle = 30, 30 averages, 10 slices, 1-mm slice thickness). MRI measuring time was ~10 minutes with the total anesthesia time (that includes positioning, adjustments, and acquisition of anatomical images) approaching 30 minutes. Since several studies demonstrated that a long anesthesia period effects body organs such as the heart and brain in rodents (38–40), anesthesia was kept at short as possible, making the use of three-dimensional (3D) higher spatial resolution acquisition with comparable SNR difficult. At the end of the MRI measurements, rats were allowed to recover before being sent back to the animal facility.

After MRI measurements, 6-OHDA lesioned rats were perfused through the aorta, first with physiological saline and second with 4% paraformaldehyde by hydrostatic pressure. To assess the degree of dopaminergic neuron depletion in the BG pathway, tyrosine hydroxylase (TH) immunofluorescent staining (rabbit immunoglobulin G [IgG] 1:100, Chemicon, Temecula, USA) was performed on two 20-μm coronal frozen sections of the striatum. Staining intensity was measured using Adobe PhotoShop 6.0 software and the lesioned side was compared to the intact side for determination of lesion severity in individual animals. Only 18 rats that were found to have a pronounced reduction (above 60%) in TH expression in the striatum of the lesioned side as compared to the nonlesioned side were included in this study. Another method that was used to assess the behavioral outcome of dopaminergic neuron depletion in the 6-OHDA rats was the turning behavior test. It was previously demonstrated that due to the imbalance in the dopamine levels between the healthy and the lesioned hemisphere, the rate of the rotations the 6-OHDA rats exhibit following systemic administration of dopamine agonist or antagonist, is directly related to the dopaminergic lesion severity (41). The rate of rotations after apomorphine (dopamine agonist) injection (2 mg/kg subcutaneously [s.c.]; Sigma) was measured in 10 of the 6-OHDA rats for 60 minutes after MRI measurements. All these rats exhibited significant turning behavior (>6 rotations/minute) (41), which indicates a massive loss of dopaminergic neurons.

All image analysis was carried out using custom-written IDL (Interactive Data Language, Research Systems, Boulder, CO, USA) software developed in-house. The Paxinos and Watson (36) rat brain atlas was digitized, and overlaid on the corresponding MRI images to aid in selecting the appropriate regions of interest (ROIs). The ROIs were then selected in two different ways: first, ROIs were selected for each individual animal independently; second, images from all animals were registered using IDL 2D registration procedure and ROIs were selected only on the reference image. Since no significant differences were observed between these two analyses, the results presented are from the former analysis. The signal intensity in the ROIs was averaged and the percentage difference from the images before manganese injection was calculated. To correct for possible variation in signal intensity between the different measurements performed on different days, images were normalized according to the right muscular area outside the brain where no $Mn^{2+}$ accumulation is expected or observed. Paired Student's two tailed *t*-test statistics within groups (the same ROI at different time-points or between ROIs) and unpaired two tailed *t*-test across groups was used to assess significant signal increase.

The ROIs that were selected for the SN manganese injection were: the anteroventral thalamic nucleus (AV; 70 pixels), Hab complex (35 pixels) and the sensorimotor cortex (710 pixels) of the two hemispheres (total six ROIs), together with the right visual cortex area (650 pixels) that was used as a control. For the EP injection, the same ROIs were used except for the thalamic relay nuclei due to its proximity to the injection site. For the Hab injection, two ROIs were chosen at the interpeduncular (IP) and the raphe nuclei.

## RESULTS

Figure 1 shows the average signal time course for the PD and sham-operated rats at the four ROIs as a result of $MnCl_2$ injection to the EP. Examples of MEMRI images taken 24-hour postinjection are also shown. Note that for easier visualization of signal enhancements these images, as well as images in the other figures, are independently scaled. Significant ipsi- and contralateral signal increase were observed in the Hab at 24 hours and 48 hours postinjection in both PD and control groups when compared with baseline ($P < 0.05$). There was significantly higher signal increases (at 24 hours and 48 hours) in the PD rat group in both ipsi- and contralateral Hab ($P < 0.05$, Fig. 1a). Significant signal increase compared to baseline was observed in the sensorimotor cortex (Fig. 1b) 24 hours and 48 hours postinjection, with significantly higher increase in the sham-operated group ($P < 0.05$). No signal increase was observed in the contralateral sensorimotor cortex.

Figure 2 shows the results of $MnCl_2$ injections to the SN area. Significant signal increase was observed in the PD rat group 3 hours postinjection in both ipsi- and contralateral AV ($P < 0.05$) with no corresponding increases in the sham-operated group (Fig. 2a). No signal increase was observed at later times. In the Hab (Fig. 2b), significant signal enhancement ($P < 0.05$) ipsi- and contralateral to the injection site was observed 24 hours postinjection, with no corresponding signal change in the sham-operated rat group. At 48 hours postinjection both the PD and sham-operated groups exhibited significant signal increase in the ipsilateral Hab ($P < 0.05$). No significant signal changes were found in the sensorimotor cortex in both groups.

Figure 3 shows the results of $MnCl_2$ injections to the Hab area. As early as three hours after injection significant signal increases in the IP were observed in the sham-operated rats as compared to baseline. In contrast, IP signal enhancement in the PD rats reached its maximum at 24 hours postinjection ($P < 0.05$). In addition, significant signal increases in the raphe nucleus (Fig. 3b) were observed at 24 hours postinjection in the 6-OHDA group ($P < 0.05$) with no change in the control group.

To test whether signal enhancement is independent on anatomical connections, a control area in the visual cortex was selected since it does not have direct connections with the EP, SN, or the Hab complex. As expected, no $Mn^{2+}$ induced signal enhancement in this area was observed in any of the groups at any time-point postinjection following EP, SN, or Hab injections ($P > 0.5$).

## DISCUSSION

The longitudinal study presented here and in particular the proximity of the acquisition to the manganese injection operation, required special care with regard to animal health conditions to minimize mortality. Multiple long anesthetic periods increase animal mortality

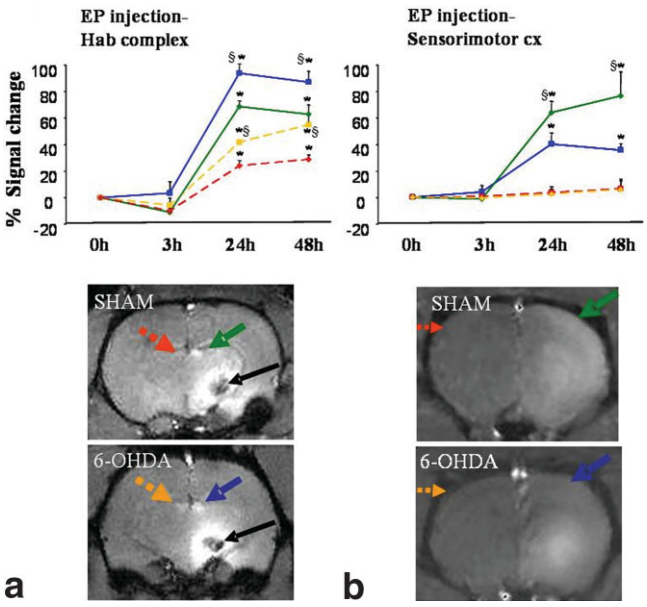


**Figure 1.** Percentage signal change following manganese injection to the entopeduncular nucleus (EP). Top panel: Percentage signal change (with +1 mean standard error) before, 3, 24, and 48 hours after injection to the EP in the habenula complex (Hab) (**a**) and the sensorimotor cortex (**b**) areas in the sham-operated (SHAM, $N = 6$) and 6-OHDA model rats ($N = 6$) (green and dashed-red for SHAM lesioned and nonlesioned hemispheres, respectively; blue and dashed-orange for 6-OHDA lesioned and nonlesioned hemispheres, respectively; $^*P < 0.05$ signal vs. baseline; §$P < 0.05$ SHAM vs. 6-OHDA). Bottom panels: typical MRI 24 hours after manganese injection. Beside the injection site (black arrow), enhanced $Mn^{2+}$ accumulation is seen (bright areas) in the ipsi- and contralateral Hab (a) and decreased $Mn^{2+}$ accumulation is observed in the ipsilateral sensorimotor cortex in the Parkinson's disease model rats compared to sham-operated rats (b).

and can create irregular physiological conditions that might affect image signal intensity. Due to these reasons, effort was made to minimize the time that the animals were kept under anesthesia. To obtain an SNR that allows observing signal enhancement as low as ~10% with total anesthetic time ≤30 minutes, 2D rather than 3D acquisition was used. Our other health concern was that long-term exposure to manganese can cause neurological disorders whose symptoms are similar to Parkinsonism (42). However, animal studies have demonstrated that a single dose (29) or repetitive administrations of $MnCl_2$ (43) do not produce such symptoms in spite of the fact that in some cases an increase in manganese concentration in BG nuclei was observed 24 hours after the first manganese administration (44). Therefore, we assume that the low dose of injected manganese did not create any neurological effect particularly during the 48 hours of our measurements.

Major concerns in the MEMRI method used in this study are: 1) the difficulty of differentiating between the effect of passive diffusion and anterograde neuronal transport; and 2) comparisons between the efficiency of different neuronal connections due to possible dependence on manganese transfer affinity. To address these difficulties we have adopted the differential approach. Namely, we compare signal enhancements of nuclei pair (injection site and chosen ROI) between control and 6-OHDA groups. Additionally, nuclei proximate to injection sites or nuclei whose signal enhancement is not clearly separated from signal enhancement in the injection site, are not used in the analysis.

In the discussion below we assume that: 1) the signal enhancement induced by manganese is related to the amount of manganese concentration (45); and 2) manganese accumulation and its time-course are indicative of the connectivity between injection and target sites (46,47). Within these assumptions, the term "connectivity" is used repetitively below.

A good example of the strength and significance of MEMRI is our results' congruence with the expected changes in BG-cortex circuitry in the parkinsonian state. The classical BG-cortex circuitry models predict that following dopaminergic cell loss in the SNc, the BG output nuclei receive more excitatory input, resulting in their increased inhibitory output (to the thalamus relay nuclei), followed by decreased cortical activity. While other neuroimaging studies have not observed decreased primary motor activation in PD patients (48) or in a rat model of PD (49), our results suggest that reduced BG-sensorimotor connectivity in PD is proba-

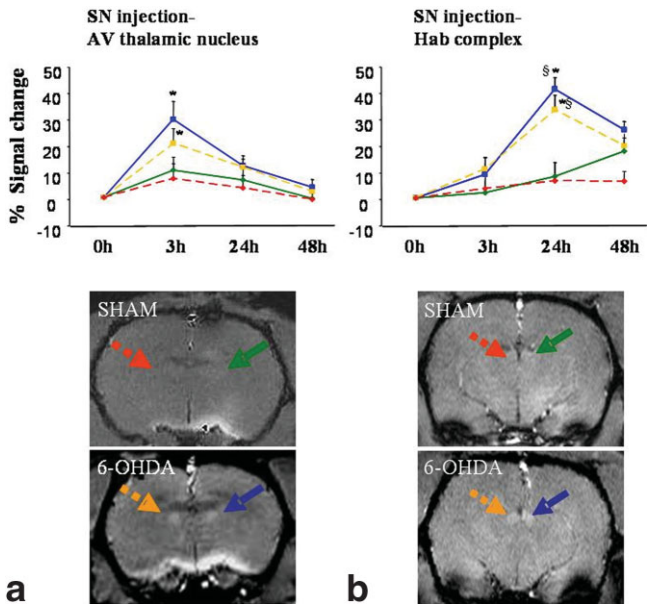


**Figure 2.** Percentage signal change following manganese injection to the substantia nigra (SN). Top panel: Percentage signal change (with +1 mean standard error) before, 3, 24, and 48 hours after injection to the SN in the anteroventral (AV) thalamic nucleus (**a**) and habenular complex (Hab) (**b**) areas in the sham-operated (SHAM, $N = 6$) and 6-OHDA model rats ($N = 6$) (green and dashed-red for SHAM lesioned and nonlesioned hemispheres, respectively; blue and dashed-orange for 6-OHDA lesioned and nonlesioned hemispheres, respectively; $^*P < 0.05$ signal vs. baseline; §$P < 0.05$ SHAM vs. 6-OHDA). Bottom panels: typical MRI 3 hours (a) and 24 hours (b) after $MnCl_2$ injection. Enhanced $Mn^{2+}$ accumulation is seen in the ipsi- and contralateral AV thalamic nucleus (a) and Hab (b) in the Parkinson's disease model rats compared to sham-operated rats.

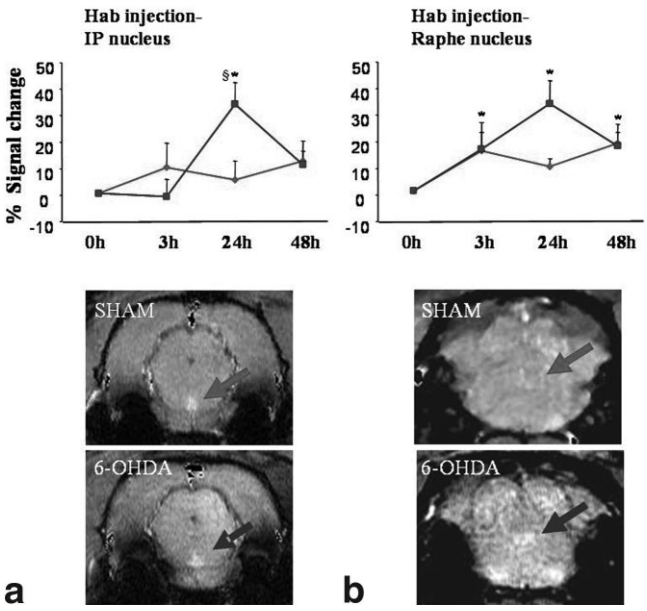


**Figure 3.** Percentage signal changes following manganese injection to the habenular complex (Hab). Top panel: Percentage change (with +1 mean standard error) before, 3, 24, and 48 hours after injection to the Hab in the interpeduncular nucleus (IP) (**a**) and in the raphe nucleus (**b**) (green sham-operated [SHAM, $N = 6$]; blue 6-OHDA $N = 6$; $^*P < 0.05$ signal vs. baseline; §$P < 0.05$ SHAM and 6-OHDA difference). Bottom panels: typical MRI of SHAM and 6-OHDA rats taken 24 hours after $MnCl_2$ injection. Significant enhanced $Mn^{2+}$ accumulation was found in the IP (a) and the raphe nucleus (b) 24 hours postinjection in the 6-OHDA compared to sham-operated rats. [Color figure can be viewed in the online issue, which is available at www.interscience.wiley.com.]

bly a consequence of the reduced thalamus-cortex connectivity. Figure 1b shows the decreased sensorimotor cortex signal after $MnCl_2$ injection to the EP area and Fig. 2a shows the increase AV thalamic nucleus signal after $MnCl_2$ injection to the SN. This suggests that the sensorimotor cortex signal decrease was mediated through the enhanced EP-thalamic functional (inhibitory) connectivity. Unfortunately, the proximity of the thalamic area to the EP has prohibited us from drawing any significant conclusions regarding changes in the thalamic signal intensity following EP $MnCl_2$ injection. This agreement with classical model predictions, strengthens our view for the validity of the MEMRI results in our PD/control comparison.

One of the motivations of this study was to test the hypothesis of bilateral BG connectivity (47) originated by reports of bilateral abnormal cortical responses and resting state fluctuations in the unilateral model of PD (16,41,50) and in hemiparkinsonian patients (15). The findings of strong bilateral connections from the BG output nuclei to the AV thalamic nucleus and to the Hab complex strongly support the idea of bilateral connectivity that is not mediated by the cortex (16). However, one could claim that the bilateral connectivity from the BG output nuclei to the Hab complex, observed in the 6-OHDA rat group, could be explained by bilateral Hab connectivity and not by bilateral BG-Hab connectivity. However, since there are very few neurons in the lateral Hab and none in the medial Hab with contralateral projections within the habenular commissure (51), and since there were equivalent temporal patterns of the signal increases in the right and the left Hab complexes following manganese injection to the SN area (Fig. 2a), this favors the latter explanation of enhanced bilateral BG projections (19,20).

Another goal of this study was to test whether the loss of dopamine in the SNc affects the effective connectivity between different limbic structures. The significant signal enhancement in the Hab complex as a results of manganese injection to the BG output nuclei on one hand and the stronger signal enhancement in 6-OHDA rats on the other hand, suggest that the Hab complex is linked to BG circuit in healthy and in parkinsonian-like states, which was shown for the former in primates (23). The signal enhancement in the IP and in the raphe nuclei in the 6-OHDA rat group after manganese injection to the Hab, suggest enhanced connectivity from the Hab to these nuclei and that this connectivity is probably mediated by the enhanced BG-Hab connections. Of particular interest is the involvement of the raphe nucleus since it generates most of the brain's serotonin (5-HT), which is known to modulate mood, emotion, sleep, and appetite. Evidence for the involvement of 5-HT dysfunction in PD depression (52–55) and in non-PD depressed patients (56), including the fact that more than 40% of PD patients suffer from depression and mood disorders in addition to their motor disorders (57,58), support the notion that the serotonin system is involved in PD. The ventral striatum, including the nucleus accumbens, in which an interaction between the 5-HT and the dopaminergic systems is known to exist, was suggested as a possible pathway connecting dopaminergic and serotonergic systems, thus modulating dopamine and 5-HT release in PD (59). Here, we propose that the linkage between these two systems is taking place through the Hab complex: The overactivation of the Hab complex by the BG output nuclei increases its inhibitory γ-aminobutyric acid (GABA) output (60–62) to both the raphe and the IP nuclei, reducing 5-HT synthesis in the raphe nucleus.

Incorporating known anatomical connections with our findings, we propose to extend the classical box-and-arrow model of the BG-cortex circuitry by linking it to a limbic circuit. Indeed, little is known about the complex molecular and the network mechanisms linking these two circuits and, in particular, the modifications they can undergo during pathological states. Although this extension is based on limited data and clearly additional different experiments are needed, the proposed circuit points out that alteration in one neuronal circuit (BG) affects the other (limbic). For simplicity, the cortex-BG-cortex circuit of the diagram (Fig. 4, right side) uses the classical view and no attempt has been made to include more recent views. The shaded area in the diagram symbolizes the new limbic circuit whereas the classical cortex-BG-cortex circuit is shown in the bright (right) side. Black and white arrows are inhibitory and excitatory projections, respectively, while arrow width represents projection efficiency. Consider first the healthy brain: as in the classical view, the cortex sends excitatory input to the striatum, which in

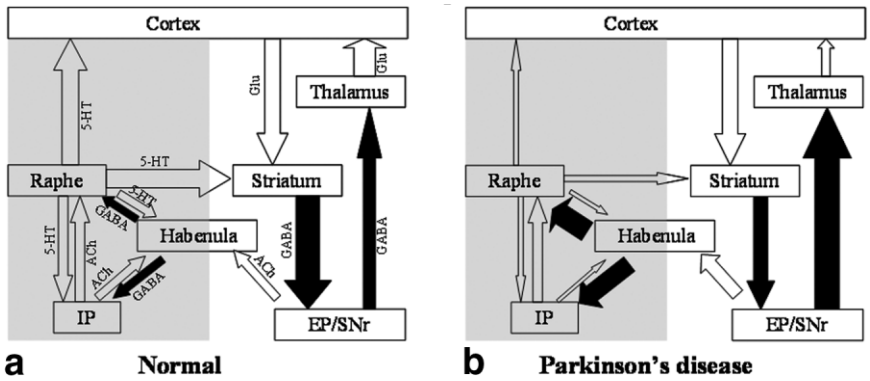


**Figure 4.** The BG-limbic model. Left: normal brain. Right: Parkinson's disease brain. The bright area (right side of each diagram) represents the classical model of basal ganglia-cortex circuitry while the gray area (left side of each diagram) presents the additional limbic part with the habenular complex the linking structure between the two. White/black arrows stand for excitatory/inhibitory projections and arrow width illustrates projection efficacy. The neurotransmitters involved are written in the left diagram. (entopeduncular nucleus (EP), substantia nigra (SN), interpeduncular nucleus (IP), acetylcholine (ACh), serotonin (5-HT), γ-aminobutyric acid (GABA)).

turn projects to the BG output nuclei, the EP and SNr. The EP and the SNr project to the thalamic nuclei, which send afferent excitatory GABAergic projections to the cortex. The extended view includes EP projections to the Hab that are mainly cholinergic, arising from a different cell population (63,64). The Hab receives excitatory afferents from the IP and the raphe nuclei (65,66), and sends mainly inhibitory input back to these nuclei (60–62), although messenger ribonucleic acid (mRNA) of nicotinic acetylcholine (ACh) receptors was found in the Hab as well (67). The raphe nucleus, which receives afferent projections from diverse brain regions, including the IP and the Hab, sends excitatory serotonergic projections to the striatum, SNc, cortex, septum, Hab, and IP, as well as to many other limbic regions (22,62,65,66). In the PD state, in line with the classical model, the BG output nuclei receive less inhibitory input from the striatum, thus overactivation results in more GABAergic projections to the thalamus, reducing the excitatory thalamocortical projections. The extended view includes stronger cholinergic projections from the overactivated output nuclei of the BG to the Hab. Previous studies using 2-Deoxyglucose (2-DG) methods demonstrated that the Hab is overactivated in 6-OHDA rats not treated with L-dopamine (L-DOPA) (24) and also in depressed animals (68). According to the proposed circuit, this overactivation is the result of a stronger projection from the BG output nuclei. The overactivation of the Hab complex in turn, increases the inhibitory Hab output to both raphe and IP nuclei, thus affecting the 5-HT synthesis in the raphe nucleus. This results in a reduction of the excitatory output to limbic nuclei as well as to the striatum and the cortex, from the raphe and the IP nuclei. Future experiments will aid in elucidating the exact mechanisms that contribute to the alterations in the BG-limbic effective connectivity during PD.

In summary, these results point to two main differences between control and Parkinsonian rats. The first is the strengthening of the BG and the contralateral (nonlesioned) hemisphere's connections in the Parkinsonian state, which is supported by the observation of the bilateral signal enhancement in the Habenula complex (following injections in the SN and EP areas ) and the thalamic anteroventral (following SN area injection). The second is the Habenula complex involvement in PD and its possible modulation on the 5-HT level that can account for patient symptoms of mood disorder in addition to the expected motor ones. Our results suggest that the Habenula complex plays a significant role in PD and its enhanced connectivity with the raphe nucleus suggest that it might be involved in the pathogenesis of the emotional (limbic) symptoms of PD.

## ACKNOWLEDGMENTS

We thank Dr. Alan P. Koretsky for stimulating discussions and comments on the manuscript.

## REFERENCES

1. Schultz W. Dopamine neurons and their role in reward mechanisms. Curr Opin Neurobiol 1997;7:191–197.
2. Wise RA. Drug-activation of brain reward pathways. Drug Alcohol Depend 1998;51:13–22.
3. Jog MS, Kubota Y, Connolly CI, Hillegaart V, Graybiel AM. Building neural representations of habits. Science 1999;286:1745–1749.
4. Stevens JR. An anatomy of schizophrenia? Arch Gen Psychiatry 1973;29:177–189.
5. Menon V, Anagnoson RT, Glover GH, Pfefferbaum A. Functional magnetic resonance imaging evidence for disrupted basal ganglia function in schizophrenia. Am J Psychiatry 2001;158:646–649.
6. Koob GF, Nestler EJ. The neurobiology of drug addiction. J Neuropsychiatry Clin Neurosci 1997;9:482–497.
7. Breiter HC, Rauch SL, Kwong KK, et al. Functional magnetic resonance imaging of symptom provocation in obsessive-compulsive disorder. Arch Gen Psychiatry 1996;53:595–606.
8. Albin RL, Young AB, Penney JB. The functional anatomy of basal ganglia disorders. Trends Neurosci 1989;12:366–375.
9. DeLong MR. Primate model of movement disorders of the basal ganglia origin. Trends Neurosci 1990;13:281–285.
10. Middleton FA, Strick PL. Basal-ganglia 'projections' to the prefrontal cortex of the primate. Cereb Cortex 2002;12:926–935.
11. Joel D, Weiner I. The connections of the primate subthalamic nucleus: indirect pathways and the open-interconnected scheme of basal ganglia-thalamocortical circuitry. Brain Res Rev 1997;23:62–78.
12. Bar-Gad I, Bergman H. Stepping out of the box: information processing in the neural networks of the basal ganglia. Curr Opin Neurobiol 2001;11:689–695.

13. Joel D, Weiner I. The organization of the basal ganglia-thalamocortical circuits: open interconnected rather than closed segregated. Neuroscience 1994;63:363–379.
14. Bar-Gad I, Havazelet-Heimer G, Goldberg JA, Ruppin E, Bergman H. Reinforcement-driven dimensionality reduction—a model for information processing in the basal ganglia. J Basic Clin Physiol Pharmacol 2000;11:305–320.
15. Thobois S, Dominey P, Decety J, Pollak P, Gregoire MC, Broussolle E. Overactivation of primary motor cortex is asymmetrical in hemiparkinsonian patients. Neuroreport 2000;11:785–789.
16. Pelled G, Bergman H, Goelman G. Bilateral overactivation of the sensorimotor cortex in the unilateral rodent model of Parkinson's disease—a functional magnetic resonance imaging study. Eur J Neurosci 2002;15:389–394.
17. Pritzel M, Sarter M, Morgan S, Huston JP. Interhemispheric nigrostriatal projections in the rat: bifurcating nigral projections and loci of crossing in the diencephalon. Brain Res Bull 1983;10:385–390.
18. Morgan S, Huston JP. The interhemispheric projection from the substantia nigra to the caudate-putamen as depicted by the anterograde transport of [3H]leucine. Behav Brain Res 1990;38:155–162.
19. Parent A, Hazrati LN. Functional anatomy of the basal ganglia. I. The cortico-basal ganglia-thalamo-cortical loop. Brain Res Rev 1995;20:91–127.
20. Gerfen CR, Wilson CJ. The basal ganglia. In: Swanson LW, Björklund A, Hokfelt T, editors. In: Handbook of chemical neuroanatomy, New York: Elsevier Science; 1996. p 371–468.
21. Sutherland RJ. The dorsal diencephalic conduction system: a review of the anatomy and functions of the habenular complex. Neurosci Biobehav Rev 1982;6:1.
22. Ellison G. Stimulant-induced psychosis, the dopamine theory of schizophrenia, and the habenula. Brain Res Brain Res Rev 1994; 19:223–239.
23. Saleem KS, Pauls JM, Augath M, et al. Magnetic resonance imaging of neuronal connections in the macaque monkey. Neuron 2002;34: 685–700.
24. Trugman JM, Wooten GF. The effects of L-DOPA on regional cerebral glucose utilization in rats with unilateral lesions of the substantia nigra. Brain Res 1986;379:264–274.
25. Pautler RG, Silva AC, Koretsky AP. In vivo neuronal tract tracing using manganese-enhanced magnetic resonance imaging. Magn Reson Med 1998;40:740–748.
26. Koretsky AP, Silva AC. Manganese-enhanced magnetic resonance imaging (MEMRI). NMR Biomed 2004;17:527–531.
27. Lee JH, Koretsky AP. Manganese enhanced magnetic resonance imaging. Curr Pharm Biotechnol 2004;5:529–537.
28. Lin YJ, Koretsky AP. Manganese ion enhances T1-weighted MRI during brain activation: an approach to direct imaging of brain function. Magn Reson Med 1997;38:378.
29. Saleem KS, Pauls JM, Augath M, et al. Magnetic resonance imaging of neuronal connections in the macaque monkey. Neuron 2002;34: 685.
30. Van Der Linden A, Verhoye M, Van Meir V, et al. In vivo manganese-enhanced magnetic resonance imaging reveals connections and functional properties of the songbird vocal control system. Neuroscience 2002;112:467.
31. Van Meir V, Pavlova D, Verhoye M, et al. In vivo MR imaging of the seasonal volumetric and functional plasticity of song control nuclei in relation to song output in a female songbird. Neuroimage 2006; 31:981–992.
32. Yu X, Wadghiri YZ, Sanes DH, Turnbull DH. In vivo auditory brain mapping in mice with Mn-enhanced MRI. Nat Neurosci 2005;8: 961–968.
33. Angenstein F, Niessen HG, Goldschmidt J, et al. Manganese-enhanced MRI reveals structural and functional changes in the cortex of Bassoon mutant mice. Cereb Cortex 2007;17:28–36.
34. Thuen M, Singstad TE, Pedersen TB, et al. Manganese-enhanced MRI of the optic visual pathway and optic nerve injury in adult rats. J Magn Reson Imaging 2005;22:492–500.
35. Murayama Y, Weber B, Saleem KS, Augath M, Logothetis NK. Tracing neural circuits in vivo with Mn-enhanced MRI. Magn Reson Imaging 2006;24:349–358.
36. Paxinos G, Watson C. The rat brain in stereotaxic coordinates, 2nd edition. New York: Academic Press; 1986. 237 p.
37. Pautler RG, Silva AC, Koretsky AP. In vivo neuronal tract tracing using manganese-enhanced magnetic resonance imaging. Magn Reson Med 1998;40:740.
38. Iltis I, Kober F, Dalmasso C, Lan C, Cozzone PJ, Bernard M. In vivo assessment of myocardial blood flow in rat heart using magnetic resonance imaging: effect of anesthesia. J Magn Reson Imaging 2005;22:242–247.
39. Mills CD, Robertson CS, Contant CF, Henley CM. Effects of anesthesia on polyamine metabolism and water content in the rat brain. J Neurotrauma 1997;14:943–949.
40. Wood AK, Klide AM, Pickup S, Kundel HL. Prolonged general anesthesia in MR studies of rats. Acad Radiol 2001;8:1136–1140.
41. Schwarting RK, Huston JP. Unilateral 6-hydroxydopamine lesions of meso-striatal dopamine neurons and their physiological sequelae. Prog Neurobiol 1996;49:215–266.
42. Calne DB, Chu NS, Huang CC, Lu CS, Olanow W. Manganism and idiopathic parkinsonism: similarities and differences. Neurology 1994;44:1583–1586.
43. Baek SY, Lee MJ, Jung HS, et al. Effect of manganese exposure on MPTP neurotoxicities. Neurotoxicology 2003;24:657–665.
44. Dodd CA, Ward DL, Klein BG. Basal ganglia accumulation and motor assessment following manganese chloride exposure in the C57BL/6 mouse. Int J Toxicol 2005;24:389–397.
45. Chuang KH, Koretsky A. Improved neuronal tract tracing using manganese enhanced magnetic resonance imaging with fast T(1) mapping. Magn Reson Med 2006;55:604–611.
46. Van der Linden A, Van Meir V, Tindemans I, Verhoye M, Balthazart J. Applications of manganese-enhanced magnetic resonance imaging (MEMRI) to image brain plasticity in song birds. NMR Biomed 2004;17:602–612.
47. van der Zijden JP, Wu O, van der Toorn A, Roeling TP, Bleys RL, Dijkhuizen RM. Changes in neuronal connectivity after stroke in rats as studied by serial manganese-enhanced MRI. Neuroimage 2007;34:1650–1657.
48. Sabatini U, Boulanouar K, Fabre N, et al. Cortical motor reorganization in akinetic patients with Parkinson's disease: a functional MRI study. Brain 2000;123(Pt 2):394–403.
49. Pelled G, Bergman H, Goelman G. Bilateral overactivation of the sensorimotor cortex in the unilateral rodent model of Parkinson's disease—a functional magnetic resonance imaging study. Eur J Neurosci 2002;15:389–394.
50. Pelled G, Bergman H, Ben-Hur T, Goelman G. Reduced basal activity and increased functional homogeneity in sensorimotor and striatum of a Parkinson's disease rat model: a functional MRI study. Eur J Neurosci 2005;21:2227–2232.
51. Araki T, Tanji H, Kato H, Itoyama Y. Sequential changes of dopaminergic receptors in the rat brain after 6- hydroxydopamine lesions of the medial forebrain bundle. J Neurol Sci 1998;160:121–127.
52. Mayeux R, Stern Y, Cote L, Williams J. Altered serotonin metabolism in depressed patients with Parkinson's disease. Neurology 1984;34:642–646.
53. McCance-Katz EF, Marek KL, Price LH. Serotonergic dysfunction in depression associated with Parkinson's disease. Neurology 1992; 42:1813–1814.
54. Becker T, Becker G, Seufert J, et al. Parkinson's disease and depression: evidence for an alteration of the basal limbic system detected by transcranial sonography. J Neurol Neurosurg Psychiatry 1997;63:590–595.
55. Murai T, Muller U, Werheid K, et al. In vivo evidence for differential association of striatal dopamine and midbrain serotonin systems with neuropsychiatric symptoms in Parkinson's disease. J Neuropsychiatry Clin Neurosci 2001;13:222–228.
56. Smith KA, Morris JS, Friston KJ, Cowen PJ, Dolan RJ. Brain mechanisms associated with depressive relapse and associated cognitive impairment following acute tryptophan depletion. Br J Psychiatry 1999;174:525–529.
57. Anderson KE, Weiner WJ. Psychiatric symptoms in Parkinson's disease. Curr Neurol Neurosci Rep 2002;2:303–309.
58. Burn DJ. Depression in Parkinson's disease. Eur J Neurol 2002; 9(Suppl 3):44–54.
59. Alexander GE, Crutcher MD, DeLong MR. Basal ganglia-thalamocortical circuits: parallel substrates for motor, oculomotor, "prefrontal" and "limbic" functions. Prog Brain Res 1990;85: 119–146.

60. Wang RY, Aghajanian GK. Physiological evidence for habenula as major link between forebrain and midbrain raphe. Science 1977; 197:89–91.
61. Nishikawa T, Fage D, Scatton B. Evidence for, and nature of, the tonic inhibitory influence of habenulointerpeduncular pathways upon cerebral dopaminergic transmission in the rat. Brain Res 1986;373:324–336.
62. Kalen P, Strecker RE, Rosengren E, Bjorklund A. Regulation of striatal serotonin release by the lateral habenula-dorsal raphe pathway in the rat as demonstrated by in vivo microdialysis: role of excitatory amino acids and GABA. Brain Res 1989;492:187–202.
63. Kha HT, Finkelstein DI, Pow DV, Lawrence AJ, Horne MK. Study of projections from the entopeduncular nucleus to the thalamus of the rat. J Comp Neurol 2000;426:366–377.
64. Moriizumi T, Hattori T. Choline acetyltransferase-immunoreactive neurons in the rat entopeduncular nucleus. Neuroscience 1992; 46:721–728.
65. Hamill GS, Jacobowitz DM. A study of afferent projections to the rat interpeduncular nucleus. Brain Res Bull 1984;13:527–539.
66. Morley BJ. The interpeduncular nucleus. Int Rev Neurobiol 1986; 28:157–182.
67. Deutch AY, Holliday J, Roth RH, Chun LL, Hawrot E. Immunohistochemical localization of a neuronal nicotinic acetylcholine receptor in mammalian brain. Proc Natl Acad Sci USA 1987;84:8697–8701.
68. Caldecott-Hazard S, Mazziotta J, Phelps M. Cerebral correlates of depressed behavior in rats, visualized using 14C-2-deoxyglucose autoradiography. J Neurosci 1988;8:1951–1961.